ACS APPLIED MATERIALS & INTERFACES

www.acsami.org

Research Article

Large Capacity Enhancement of Carbon Electrodes by Solution Processing for High Density Energy Storage

Anna K. Farquhar, Scott R. Smith, Colin Van Dyck, and Richard L. McCreery*

Cite This: *ACS Appl. Mater. Interfaces* 2020, 12, 10211−10223

Read Online

ACCESS | Metrics & More | Article Recommendations | Supporting Information

ABSTRACT: An inexpensive, solution phase modification of flat carbon electrodes by electrochemical reactions of a 1,8-diaminonaphthalene derivative results in a 120- to 700-fold increase in capacity by formation of a 15−22 nm thick organic film. Modification of high surface area carbon electrodes with the same protocol resulted in a 12- to 82-fold increase in capacity. The modification layer contains 9−15% nitrogen present as −NH− redox centers that result in a large Faradaic component involving one H^+ ion for each electron. The electrodes showed no capacity loss after prolonged cycling in 0.1 M H_2SO_4 and exhibited significantly higher charge density than similar reported electrodes based on graphene and polyaniline. Investigation of the deposition conditions revealed that N-doped oligomeric ribbons are formed both by diazonium ion reduction and diaminonaphthalene oxidation, and the 1,8 isomer is essential for the large capacity increases. The capacity increase has at least three contributions: increased microscopic surface area from ribbon formation, Faradaic reactions of nitrogen-containing redox centers, and changes in ribbon conductivity resulting from polaron formation. An aqueous fabrication process was developed which both increased capacity and improved stability and was amenable to industrial production. The high charge density, low-cost fabrication, and <25 nm thickness of the diaminonaphthalene-derived films should prove attractive toward practical application on both flat surfaces and in high surface area carbon electrodes.

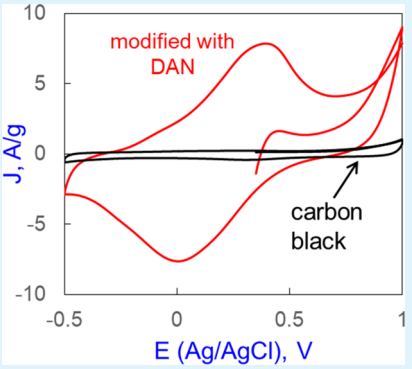

KEYWORDS: *supercapacitors, renewable energy, diazonium reduction, Faradaic energy storage, conducting polymer/carbon composites, N-doped carbon materials*

1. INTRODUCTION

Climate change and fossil fuel depletion have stimulated a substantial research effort into the development of energy storage materials that can efficiently harness energy from renewable sources such as solar and wind.[1,2] The most well-known energy storage devices are batteries, where energy is stored in chemical bonds and released via redox reactions (rechargeable batteries) or intercalation (Li ion batteries).[1] Batteries are typically characterized as having high energy density but low power density and limited stability.[3] Conversely, supercapacitors (SCs) rely on surface processes and ion motion rather than Faradaic reactions for energy storage. This permits faster charge/discharge times, increased power density, and improved cycle stability; however, the energy density of SCs tends to be orders of magnitude lower than that of batteries.[4,5] As a result, research is ongoing in the development of SC electrodes that possess energy densities comparable to those of batteries without compromising power, rate capability, and cycle life.[6]

Current commercially available SCs utilize activated carbon electrodes,[7] which store energy via electrical double layer capacitance (EDLC), enabled by the formation of an ionic double layer at the electrode/electrolyte interface. Carbon electrodes are environmentally friendly, are lightweight, and possess good EDLC properties due to their high surface area and good electrical conductivity.[3,4] To improve the capacity of carbon SCs, redox active groups can be physi- or chemisorbed to the surface.[8] Redox active materials such as RuO_2 and MnO_2 provide additional pseudocapacitance (PC) with the electrochemical signature of a capacitive electrode (linear dependence of charge stored with changing potential), but the charge storage results from electron-transfer processes.[9] Other redox active materials, including nickel and cobalt oxides/hydroxides, and conducting polymers increase the energy storage capacity of the electrodes through Faradaic reactions.[10] The Faradaic reactions increase the total energy storage capacity of the electrodes but typically suffer from reduced power density and decreased stability compared to EDLCs.[11,12] Developing carbon-based materials with covalently bonded redox active groups should enable electrode materials with the high surface area, conductivity, rate

Received: October 1, 2019
Accepted: February 10, 2020
Published: February 10, 2020

https://dx.doi.org/10.1021/acsami.9b17420
ACS Appl. Mater. Interfaces 2020, 12, 10211−10223

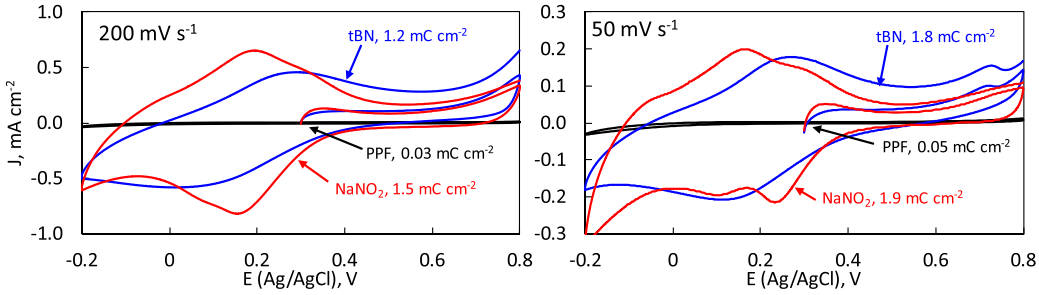

Figure 1. Voltammetry of modified PPF substrates in 0.1 M H_2SO_4, at 200 and 50 mV s^{-1}. Samples grafted with the *t*BN protocol in blue, the $NaNO_2$ protocol in red, and unmodified PPF in black. Capacity calculated by integrating area enclosed by voltammogram. Voltammetry was started at OCP (+0.3 V vs Ag/AgCl) in all cases. H_2SO_4 degassed with argon for 10 min prior to measurement.

capability, and stability characteristics of EDLC but with increased energy density.[2,7]

In previous work, we described a protocol for enhancing the capacity of both flat carbon substrates and commercially available high surface area carbon black powders.[13] A solution-based, electrochemical grafting process using 1,8-diaminonaphthalene resulted in the growth of ribbonlike structures on the carbon surfaces. A 20−100× increase in the areal capacity of flat carbon surfaces and a 10−20× increase in gravimetric capacity for high surface area carbon were observed. The capacity enhancement was partially due to a distinct Faradaic process in acidic electrolyte, possibly related to the nitrogen content in the organic film. In the current study, we have developed this grafting protocol further to establish how different grafting parameters influence the total capacity enhancement. By tuning certain fabrication parameters, both the nitrogen content and areal capacity were varied, in order to further optimize electrode performance. In addition, a more commercially attractive aqueous grafting procedure was investigated and yielded promising results on both flat and high surface area carbon materials.

2. RESULTS AND DISCUSSION

Previously, pyrolyzed photoresist films (PPFs), which are sp^2-hybridized carbon substrates with near atomic flatness, <0.5 rms roughness by atomic force microscopy (AFM),[14] and very low areal capacitance, were electrochemically modified using 1,8-diaminonaphthalene (1,8-DAN). It was proposed that treatment of an acetonitrile (ACN) solution of 1,8-DAN with *tert*-butylnitrite (*t*BN) converted the amine functional groups to diazonium moieties, which could subsequently be reduced electrochemically to a biradical that reacts with the carbon substrate to give a film of "graphenic nanoribbons".[13,15] Voltammetry in 0.1 M H_2SO_4 electrolyte showed a 41× enhancement in the voltammogram area compared to unmodified PPF (Figure 1, blue), including a large Faradaic component centered at ∼0.2 V vs Ag/AgCl. In the current work, we first investigated aqueous diazotization conditions using $NaNO_2$ in acidic solution, which has been reported as an alternative to using isolated diazonium salts or *t*BN in acetonitrile.[16−18] In addition to much lower cost, the $NaNO_2$ reaction can be conducted with an accurate 2:1 stoichiometric ratio, while *t*BN requires a higher and often variable ratio.[19] As described in detail in the experimental methods, voltammetric reduction of a 50/50 (v/v) solution of aqueous HBF_4 and ACN containing $NaNO_2$ (4 mM), 1,8-DAN (2 mM), and HBF_4 (0.05 M) on a PPF electrode followed by rinsing with ACN and immersion in 0.1 M H_2SO_4 yielded the red curves of Figure 1. Similar to the PPF surface modified with the *t*BN protocol, voltammetry shows a significant increase in the enclosed area and distinct Faradaic features. However, unlike the *t*BN layer, the voltammetry for the $NaNO_2$ layer shows two clear redox features, especially apparent at lower scan rates (Figure 1, right panel), indicating that films grafted by this protocol possess multiple redox centers. As the grafted electrodes show well-defined redox peaks in the voltammetry it is incorrect to describe them as pseudocapacitive. Capacitance (Farads) by definition is constant throughout the applied potential range, and therefore common PC materials (MnO_2 and RuO_2) give rectangular voltammograms.[9,20] Because the modified surfaces studied in this work clearly exhibit Faradaic and not purely capacitive behavior, values of capacity (Coulombs per cm^2/g) are reported, as this is the most appropriate metric for describing the charge storage performance of redox materials.[10] Additionally, the linearity of observed current vs scan rate for the *t*BN and $NaNO_2$ samples of the redox peaks and in the EDLC region at +0.6 V (Supporting Information, Figures S3 and S4) verifies that both are surface rather than diffusion controlled, unlike a traditional battery-type material.[1,21]

Constant current charge−discharge (C/D) cycling is more representative than voltammetry of how a device would operate in practice.[1] In order to determine the total capacity enhancement and the enhancement due to EDLC only, two potential ranges were recorded, one from −0.2 to +0.8 V vs Ag/AgCl to determine total capacity and a second from +0.35 to +0.65 V to measure predominantly EDLC. Figure 2A,B shows repeated C/D cycles at an applied current density of 0.1 mA cm^{-2} for bare PPF for the two potential ranges, and the indicated capacity was determined from the discharge time. As expected, C/D curves for bare PPF are triangular and weakly dependent on potential region, consistent with EDLC and a minimal Faradaic component.[21,22] After modification with 1,8-DAN using either the *t*BN (Figure 2C,D) or $NaNO_2$ (Figure 2E,F) procedures, the C/D responses for both modified PPF samples show redox features in the full −0.2 to +0.8 V range, characterized by nonlinear regions and much longer discharge times compared to bare PPF. The potentials of the nonlinear regions correspond well with the redox peaks apparent in the voltammetry of Figure 1, and capacity values calculated from the discharge time are provided in Table 1. Comparison before and after modification for the +0.35 to +0.65 V region showed an approximate 6× increase and 5× increase in EDLC for the *t*BN and $NaNO_2$ samples, respectively, indicating an increase in the ion accessible surface area available for double layer formation. The triangular shape indicates that over this

https://dx.doi.org/10.1021/acsami.9b17420
ACS Appl. Mater. Interfaces 2020, 12, 10211−10223

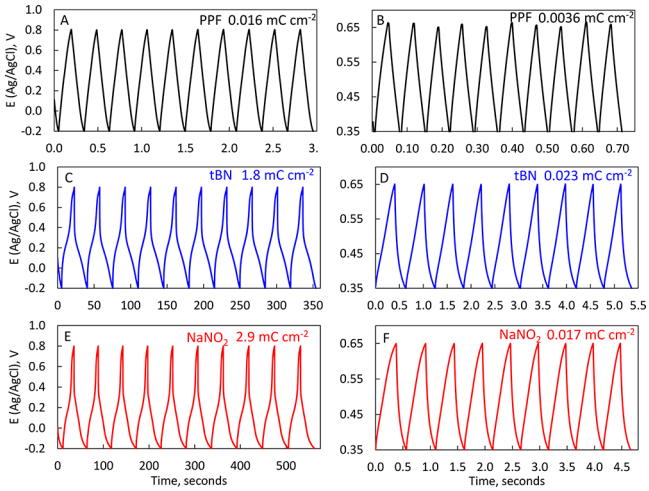

Figure 2. Constant current C/D profiles between −0.2 and +0.8 V (left) and +0.35 and +0.65 V (right) recorded at 0.1 mA cm^{-2} in 0.1 M H_2SO_4. (A, B) Bare PPF. (C, D) PPF modified by 1,8-DAN with *t*BN procedure. (E, F) PPF modified with $NaNO_2$ procedure. Capacity calculated using discharge time. H_2SO_4 degassed for 10 min with argon prior to collection.

potential region the charge storage is capacitive and not Faradaic. The total capacity over the 1 V potential window showed a remarkable 120× increase for the *t*BN sample, and an even larger 193× increase for the $NaNO_2$ sample, compared to unmodified PPF. While the increase in EDLC is significant, it represents only 2−5% of the total capacity enhancement, depending on the diazotization agent. An alternative method, based on work by Kaner et al.,[1] for determining the different contributions of each component is to calculate the capacity over small potential ranges from the 1 V C/D experiment (Supporting Information, Figure S5). The capacity was calculated from +0.7 to +0.5 V (EDLC region), and +0.1 to −0.1 V (Faradaic region). The EDLC contribution was 0.0012 mC cm^{-2} for both samples, while the PC contribution was 0.60 and 0.78 mC cm^{-2} for the *t*BN and $NaNO_2$ samples, respectively. This confirms that the Faradaic process is the primary source of the significant enhancement in charge storage capacity after modification with 1,8-DAN. Furthermore, the higher capacity enhancement for the $NaNO_2$ sample suggests that more than one redox active site is generated by this grafting protocol.

The C/D rate is an indication of power density and is often investigated by determining capacity as a function of discharge current density (Supporting Information, Figure S6). EDLC should be constant for different current densities for a flat surface, and a decrease of charge storage capacity with increasing discharge current indicates slower kinetics of either a redox process or ion motion into a porous electrode. The *t*BN grafted sample showed a 40% capacity retention after increasing the applied current density from 0.1 to 1 mA cm^{-2}, while the $NaNO_2$ grafted sample retained 45% of its initial capacity. The small improvement in the rate capability for the $NaNO_2$ sample may suggest that this grafting protocol provides a film with better ion diffusion.[23] The first three rows of Table 1 summarize the results for these samples, along with additional grafting conditions discussed below.

The electrochemical oxidation of aromatic amines, including 1,8-DAN, has been investigated previously,[25−28] often in the well-studied area of polyaniline synthesis. This raises the

Table 1. Capacity (Q) Values Calculated from Constant Current C/D Testing in 0.1 M H_2SO_4, at Increasing Current Densities (Capacity Was Calculated over the Given Potential Range Using the Discharge Time)

sample	thickness,[a] nm	Q (−0.2 to +0.8 V) J = 0.1 mA cm^{-2}, mC cm^{-2}	increase from PPF	Q (+0.35 to +0.65 V) J = 0.1 mA cm^{-2}, mC cm^{-2}	increase from PPF	Q (−0.2 to +0.8 V) J = 0.2 mA cm^{-2}, mC cm^{-2}	Q (−0.2 to +0.8 V) J = 0.4 mA cm^{-2}, mC cm^{-2}	Q (−0.2 to +0.8 V) J = 1.0 mA cm^{-2}, mC cm^{-2}
PPF		0.015		0.0036		0.018		
1,8-DAN, *t*BN (1:15)	15.8	1.8	120×	0.023	7×	1.5	1.2	0.69
1,8-DAN, $NaNO_2$ (2:1)	15.1	2.9	193×	0.016	4×	2.3	1.5	1.3
1,8-DAN, oxidative	16.9	2.6	173×	0. 036	10×	1.9	0.80	0.64
1,5 DAN, *t*BN (1:15)	1.3	0.36	27×	0.0084	2×	0.3	0.20	0.11
1,5 DAN, oxidative	2.7	0.042	3×	0.0063	2×	0.040		
1 AN, *t*BN (1:15)	2.0	0.0040	0.3×	0.0013	0.4×	0.0040		
1AN, oxidative	2.0	0.030	2×	0.0025	0.7×	0.030		
polyaniline, oxidative	2.0	0.083	6×					
mixed film	22.4	10.5	700×	0.051	14×	5.0	3.1	1.3

[a]Determined by AFM "scratching" (example in the Supporting Information, Figure S2).[24]

https://dx.doi.org/10.1021/acsami.9b17420
ACS Appl. Mater. Interfaces 2020, 12, 10211−10223

question of whether the 1,8-DAN oligomeric film is formed via the anticipated diazonium route, or via oxidation and subsequent polymerization of the amine precursor, or a combination of both routes. To investigate, 1,8-DAN-derived films were grown on PPF without the addition of *t*BN or $NaNO_2$ to the grafting solution, using identical electrochemical parameters. The voltammetry during film deposition is shown for the three cases in Figure 3, with all scans initiated in the negative direction from +0.4 V vs Ag/Ag^+, the usual conditions for diazonium reduction. Solid lines are the initial scan, and dashed lines are the 10th scan between +0.4 and −0.8 V. The small negative peak at ∼−0.25 V and noted previously[15] in the *t*BN case may be due to the expected reduction of diazonium ions generated in situ, but there is a much larger irreversible oxidation feature at approximately +0.25 V. As shown in Figure 3E, the oxidation peak is observed in the absence of *t*BN and results in the growth of a redox wave centered at ∼0.15 V that may be related to the observed redox process. The peak at +0.25 V has previously been assigned to the oxidation of the amine groups in 1,8-DAN to a cation radical species, which can subsequently be polymerized to yield a semiconducting polymer film.[29−32] Two commonly proposed structures formed with a diaminonaphthalene precursor via an oxidative rather than diazonium route are shown in Scheme 1. Whether one amine group (structure **1a**, denoted "single-point") or both amine groups (structure **2b**, "two-point") take part in this polymerization process appears to depend on the substrate and grafting conditions.[25,27] Note also that both single- and double-point binding[33,34] to the PPF surface are possible, but both should permit electron transfer between the PPF and the organic film. When both amine groups are oxidized, a nitrogen-doped graphene nanoribbon structure is grown. This result indicates that, under the *t*BN grafting conditions studied here, the oxidative grafting mechanism is significant, and the addition of *t*BN may be unnecessary to electrochemically graft films with increased capacity and a significant Faradaic component under these conditions. However, if the concentration of *t*BN in the grafting solution is increased, the grafting voltammetry (Figure 3B) shows a reduction wave from ∼0.2 to −0.2 V, no oxidation feature, and a decrease in current with repeated cycling, consistent with a diazonium grafting mechanism. This voltammetry is similar to what we have reported previously for films grafted using a *t*BN protocol and proposed to yield the graphene nanoribbon structure of Scheme 1c.[15] Furthermore, we have found that the concentration of *t*BN varies between different batches especially with age, and reliably reproducing the *t*BN concentration is problematic.

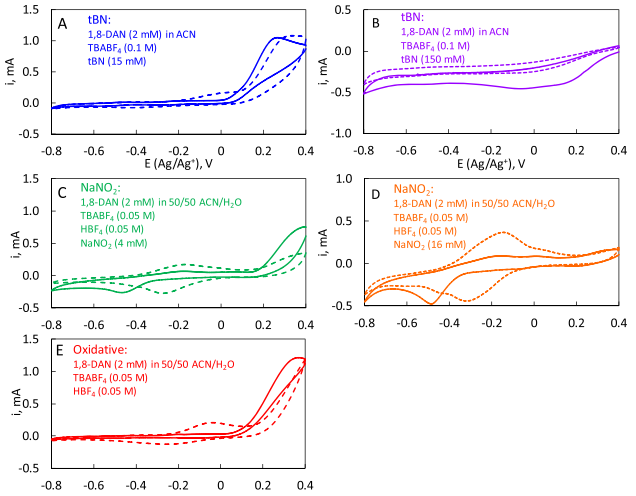

Figure 3. Grafting voltammetry for electrochemical modification of PPF with 1,8-DAN. (A, B) *t*BN protocol, (C, D) $NaNO_2$ protocol, and (E) oxidative protocol. Solution conditions provided. Scan rate = 100 mV s^{-1}. Solutions degassed with argon for 15 min prior to grafting. Solid curves are initial scans; dashed curves are 10th scans.

Scheme 1. Possible Structures for Organic Film Formed Electrochemically from 1,8-Diaminonaphthalene: 1a Single-Point Nitrogen Bridged; 2b Double-Point Nitrogen Bridged; 1c Graphene Ribbon Lacking Nitrogen; 1d Mixed Product with Both Single and Double Nitrogen Bridges

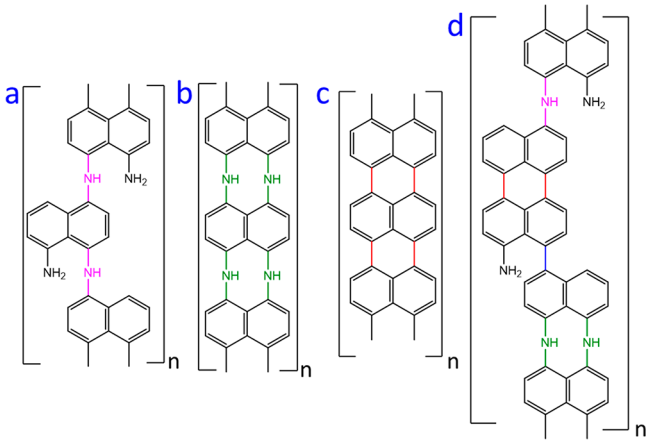

Grafting of 1,8-DAN in the presence of a 2:1 stoichiometric ratio of $NaNO_2$ in a 50/50 (v/v) ACN/aqueous acid solution differs significantly from either *t*BN or the "oxidative" conditions, as shown in Figure 3C. The grafting voltammetry for the $NaNO_2$ sample shows a reduction wave at approximately −0.45 V (vs Ag/Ag^+) on the first scan, which disappears on subsequent scans. This peak position is consistent with the reduction of aryl diazonium ions to radicals.[17,35−37] In addition, if the ratio of $NaNO_2$:1,8-DAN is increased to 8:1 (Figure 3D), the current associated with this peak increases, suggesting that a higher number of diazonium groups are available for reduction if the $NaNO_2$ concentration is increased. Unlike *t*BN, $NaNO_2$ is a stable, solid precursor, so the concentration is easily controlled. Analysis of the UV/vis absorbance (Supporting Information, Figure S7) of the grafting solution further supports the generation of an aryl diazonium ion upon addition of $NaNO_2$ to the 1,8-DAN solution. The UV/vis spectrum of 1,8-DAN acidic solution shows a peak at 223 nm and a broader peak at 286 nm. Upon addition of 2 equiv of $NaNO_2$ both peaks decrease in intensity, and new bands at 260 and 310 nm appear, consistent with the formation of the diazonium functional group.[17,38] Upon addition of 8 equiv of $NaNO_2$, the original peaks at 223 and 286 nm disappear completely, and the intensity of the 310 nm peak increases further. The UV/vis spectra and grafting voltammetry provide good evidence that primarily the diazonium grafting route is operative under the $NaNO_2$ conditions; however, whether one or both amines are involved is difficult to determine. In addition to the diazonium route, there is an irreversible oxidation wave at +0.2 V (vs Ag/Ag^+) in the 2:1 $NaNO_2$ grafting voltammetry which is similar to but

https://dx.doi.org/10.1021/acsami.9b17420
ACS Appl. Mater. Interfaces 2020, 12, 10211−10223

smaller than those observed with or without *t*BN. This suggests that the oxidative polymerization route is also active, resulting in a mixed film, such as that shown in Scheme 1d. The two mechanisms could also provide different nitrogen environments, explaining the two different redox systems seen in the H_2SO_4 voltammetry. In the 8:1 case, no oxidation wave at +0.2 V is seen, which may indicate that the higher $NaNO_2$ concentration is sufficient to convert all NH_2 groups to diazonium ions, so none remain for oxidative polymerization. Obviously, the final film structure depends on deposition conditions, which would presumably be optimized for particular applications.

Voltammetry in 0.1 M H_2SO_4 similar to that in Figure 1 was used to compare the films grafted using *t*BN (15 mM), $NaNO_2$ (4 mM), or the oxidative conditions, with the results shown in Figure 4A,B and quantitative capacity listed in Table 1. Clearly

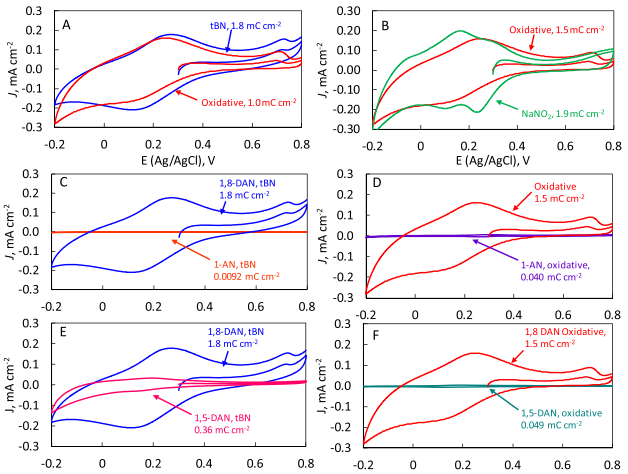

Figure 4. Voltammetry of modified PPF surfaces in 0.1 M H_2SO_4 at 50 mV s^{-1}. (A) 1,8-DAN with *t*BN (blue) and oxidative (red). (B) 1,8-DAN with $NaNO_2$ (green) and oxidative (red). (C) 1,8-DAN with *t*BN (blue) and 1-AN with *t*BN (orange). (D) 1,8-DAN oxidative (red) and 1-AN oxidative (purple). (E) 1,8-DAN with *t*BN (blue) and 1,5-DAN with *t*BN (pink). (F) 1,8-DAN oxidative (red) and 1,5-DAN oxidative (green). Capacity values calculated by integrating the area enclosed by the voltammogram. Voltammetry started at OCP (+0.3 V) in all cases. Electrolyte degassed with argon for 10 min prior to collection. Expanded versions of parts C–F provided in the Supporting Information, Figure S8. In all cases, abscissa is electrode potential relative to a Ag/AgCl electrode.

1,8-DAN is able to produce a range of film structures that enhance the charge storage capacity of the electrode, but is 1,8-DAN a prerequisite for this behavior, regardless of the grafting conditions? Figure 4C,D compares films grafted from a 1-aminonaphthalene precursor (1-AN), with and without the addition of *t*BN, with grafting voltammograms provided in the Supporting Information, Figure S1A–C. When *t*BN is present, the grafting voltammetry shows a reduction peak which disappears after the first cycle, consistent with the reduction of the diazonium ion to the aryl radical. The radical can then graft to the PPF surface forming an organic layer. The voltammetry in H_2SO_4 of this surface (Figure 5C) demonstrates a decrease in capacity compared to PPF, which agrees with reports for other monosubstituted amine precursors grafted via diazonium chemistry.[16] 1-AN can also graft oxidatively;[39,40] therefore, the grafting was repeated in the absence of *t*BN (Supporting Information, Figure S1B). Voltammetry in H_2SO_4 following grafting (Figure 5D) shows a slight increase in capacity compared to unmodified PPF (2×), but this is insignificant compared to the 173× for oxidatively grafted 1,8-DAN. Furthermore, the thickness of the 1-AN films is much lower, at 2.7 nm compared to 16.9 nm. The 1-AN electro-oxidation process has been suggested to generate dimers that are soluble in acetonitrile,[40] so they may not graft to the surface. Alternatively, this potential window may not be sufficiently positive to cause oxidation of the amine, so the positive potential limit was increased to +0.8 V (Supporting Information, Figure S1C). The grafted film provided a 13× increase in capacity, which is still significantly lower than the 1,8-DAN films. 1,5-DAN, with amine groups on opposite sides of the naphthalene unit, has voltammetry similar to 1,8-DAN using the *t*BN procedure, exhibiting an oxidative wave at approximately +0.2 V (Supporting Information, Figure S1D) consistent with literature reports for electro-oxidation.[32,41] Voltammetry of the 1,5 DAN product in H_2SO_4 is shown in Figure 4E, and the resulting film provided a 27× increase in capacity compared to unmodified PPF. 1,5-DAN was also grafted oxidatively (Supporting Information, Figure S1E), and the 0.1 M H_2SO_4 voltammetry is shown in Figure 4F. A 3× enhancement was observed, confirming that the 1,8 orientation of amine groups is required for the growth of films with large capacity enhancement. Constant current C/D cycles for the above samples are shown in the Supporting Information, Figure S9, and the resulting capacity values are summarized in Table 1. Finally, Table 1 also includes results for PPF modified by aniline oxidation, using the +0.8 to −0.8 V vs Ag/Ag^+ potential range required to form polyaniline (Figure S10). The voltammetry (Figure S11) and resulting C/D cycling (Figure S12) indicated a small increase in capacity to 0.083 mC cm^{-2}.

The voltammetry results show clearly that large increases in charge storage capacity over the potential window studied are observed using the 1,8-DAN precursor, but not for either monoaminonaphthalene or 1,5-diaminonaphthalene. Furthermore, the $NaNO_2$ procedure yields higher capacity than either *t*BN or the oxidative processes and has the additional advantage of lower cost and complexity attractive to practical applications. The relatively low long-term stability of *t*BN leads to uncertainty of its concentration during diazotization and variation in the resulting diazonium reduction voltammograms (Figure 3A,B) and in the resulting capacity. The 2:1 $NaNO_2$:1,8-DAN stoichiometry is much better defined for $NaNO_2$ compared to *t*BN, and the partially aqueous solvent reduces cost. Further optimization of the $NaNO_2$ process and elimination of acetonitrile by using water-soluble 1,8-DAN precursors is currently under investigation.

We now consider the role of nitrogen in enhancing capacity and its possible involvement in the large Faradaic component observed with the 1,8-DAN precursor. Survey X-ray photoelectron spectroscopy (XPS) results for all cases studied are provided in the Supporting Information, Figure S13, and the elemental compositions are listed in Table 2. The typical sampling depth of a few nm for XPS indicates that the substrate PPF should contribute negligibly to the atom percentage of carbon for the 12–17 nm thick organic films used for Table 2. All three preparation procedures yield significant nitrogen content, ranging from 10 to 15 atom %. This corresponds to 1.5 to 2 nitrogen atoms per naphthalene subunit in the organic films, and nitrogen was undetectable by XPS on bare PPF. There is also a measurable amount of

https://dx.doi.org/10.1021/acsami.9b17420
ACS Appl. Mater. Interfaces 2020, 12, 10211–10223

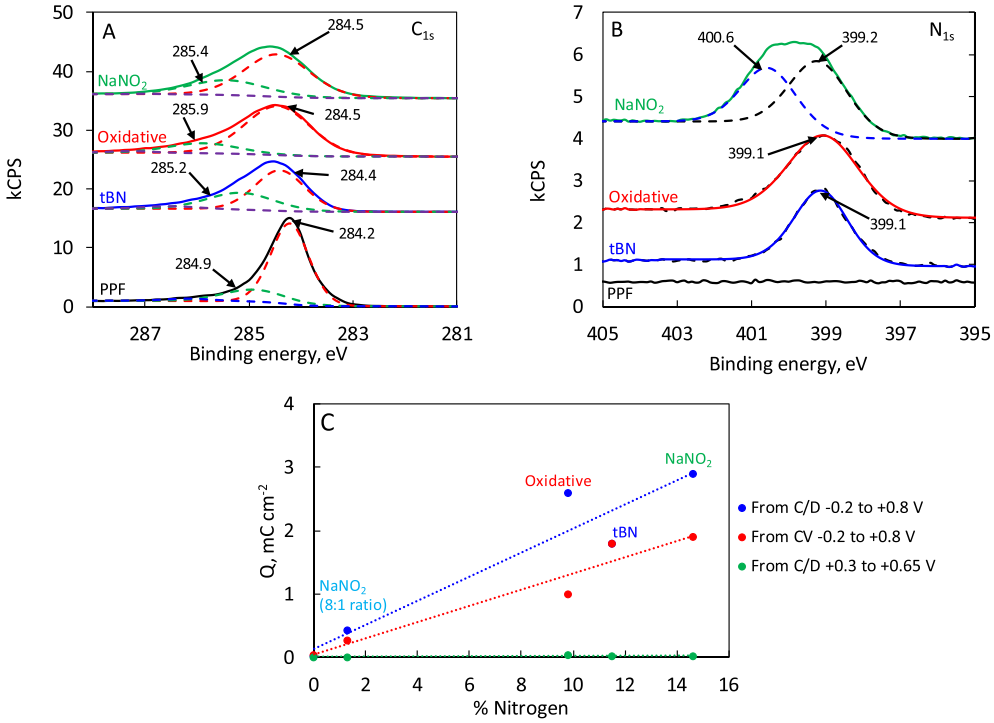

Figure 5. (A) C 1s scans for unmodified and modified PPF samples (*t*BN, oxidative, and $NaNO_2$). Spectra offset for clarity. Peak deconvolution shown. (B) N 1s scans for unmodified and modified PPF samples (*t*BN, oxidative, and $NaNO_2$). (C) Change in capacity with nitrogen atom %. Additional $NaNO_2$ sample prepared with an 8:1 ratio of $NaNO_2$ to 1,8-DAN also included as a low nitrogen example.

Table 2. XPS Results for PPF and Modified PPF Samples: *t*BN, Oxidative, and $NaNO_2$

	survey		C 1s			N 1s		
sample	element	atom %	binding energy, eV	atom %	fwhm	binding energy, eV	atom %	fwhm
PPF	carbon	97.4%	242.2	78.7%	0.86			
	oxygen	2.57%	284.9	18.9%	1.4			
			286.2	2.41%	1.0			
*t*BN	carbon	82.2%	284.4	59.3%	1.12	399.1	100%	1.6
	oxygen	3.89%	285.2	34.5%	1.52	399.1	100%	1.6
	nitrogen	11.5%	286.5	6.12%	1.31	399.1	100%	1.6
	fluorine	2.43%				399.1	100%	1.6
oxidative	carbon	80.8%	284.5	79.3%	1.4	399.1	100%	2.2
	oxygen	5.99%	285.9	18.4%	1.6	399.1	100%	2.2
	nitrogen	9.80%	287.3	2.00%	1.0	399.1	100%	2.2
	fluorine	3.55%				399.1	100%	2.2
$NaNO_2$	carbon	79.6%	284.5	70.5%	1.4	399.2	57.8%	1.8
	oxygen	5.13%	285.4	29.2%	1.7	400.6	42.2%	1.7
	nitrogen	14.6%	287.0	0.32%	0.6			
	fluorine	0.76%						

fluorine (approximately 1−4 atom %) from the tetrafluoroborate supporting electrolyte used during grafting. Residual BF_4^- ion may indicate formation of N-containing polarons during film formation, as discussed in more detail below. High resolution C 1s and N 1s scans for each sample are given in Figure 5A,B, respectively. For bare PPF, the C 1s scan shows a narrow asymmetric peak, centered at 284.2 eV, due to sp^2-hybridized carbon. A second smaller peak at 284.9 eV is also apparent in the deconvolution and is likely due to sp^3-hybridized carbon in edge and defect regions on the graphitic surface. The three modified surfaces (*t*BN, oxidative, and $NaNO_2$) show quite different spectra, with a much broader C 1s signal compared to unmodified PPF. The main contributor for all three surfaces is at 284.5 eV and is assigned to the α and β carbons of the naphthalene units.[42] An additional peak at 285.5 eV is assigned to C—N groups.[42] The N 1s scans for *t*BN and oxidative surfaces are similar, with a single peak at 399.1 eV. This is assigned to amine nitrogen (—NH—/—NH_2).[43−48] The XPS peaks for primary and secondary amines are indistinguishable,[48] so the N 1s signal for single-point (structure of Figure 4A) vs two-point binding (Figure 4B) cannot be resolved. For *t*BN the fwhm agrees with literature reports of 1.4 for —NH— in polyaniline.[45,49] In contrast, the peak for the oxidation sample is broader (fwhm = 2.2) compared to that from *t*BN, possibly due to protonation of the —NH— groups in the aqueous acid used for oxidative

https://dx.doi.org/10.1021/acsami.9b17420
ACS Appl. Mater. Interfaces 2020, 12, 10211−10223

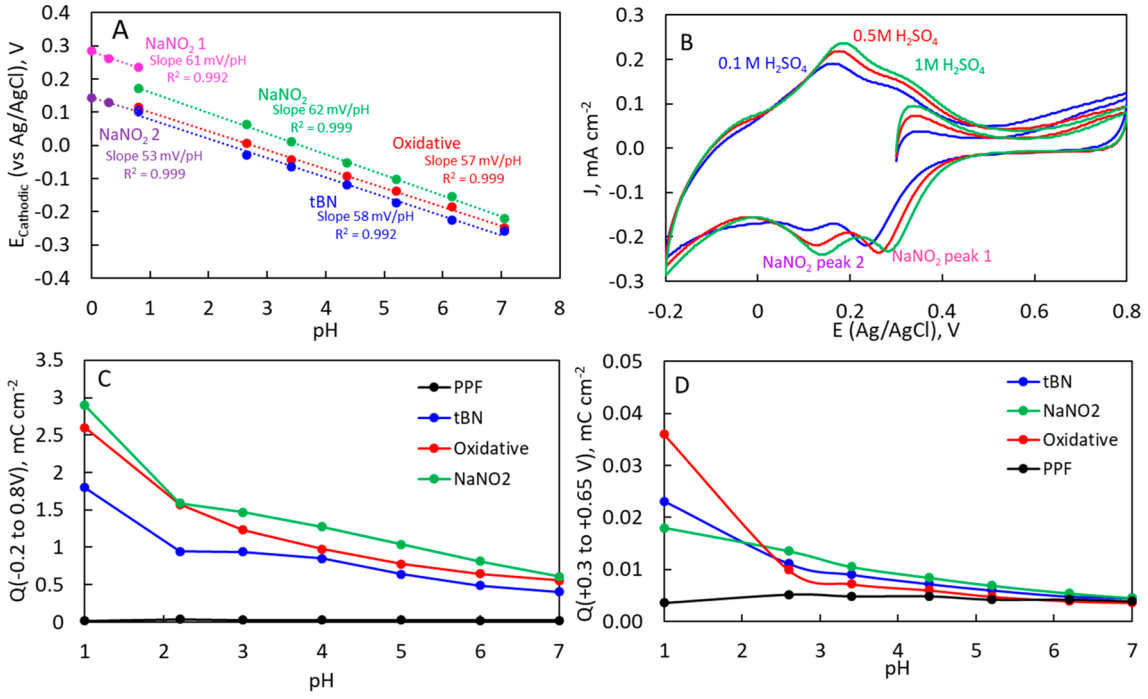

Figure 6. (A) Shift in cathodic peak potential with pH for films prepared via *t*BN (blue), oxidative (red), and $NaNO_2$ (green) protocol in McIlvaine buffer, and shift in cathodic peak potential with pH for $NaNO_2$ peaks (pink and purple) in H_2SO_4 with different concentrations. Scan rate = 50 mV s^{-1}. (B) Voltammetry at 50 mV s^{-1} for $NaNO_2$ 1,8-DAN film in H_2SO_4 at different concentrations. (C) Change in capacity (−0.2 to +0.8 V) with pH, calculated from C/D at 0.1 mA cm^{-2} in McIlvaine buffer. (D) Change in EDLC (+0.35 to +0.65 V) with pH, calculated from C/D at 0.1 mA cm^{-2} in McIlvaine buffer. pH 1 sample measured in 0.1 M H_2SO_4 in all cases.

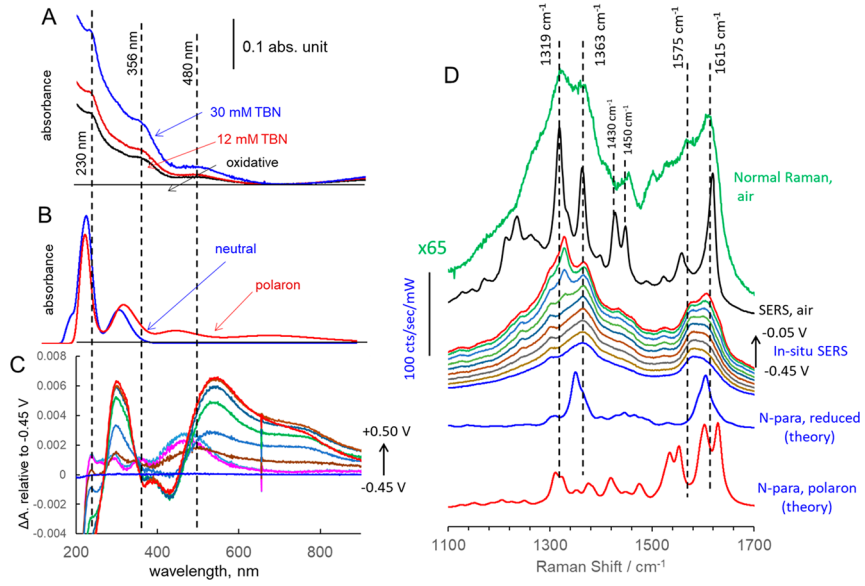

Figure 7. (A) UV−vis absorption spectra of organic films in air formed on PPF by the indicated procedures, after subtraction of the unmodified electrode spectrum. (B) Calculated spectra for neutral and polaron species with the structures in Scheme 2a. The polaron counterion was BF_4^-. (C) In situ spectra of *t*BN-modified PDF, as the change in absorbance, Δ*A*, relative to that obtained at −0.45 V vs Ag/AgCl. (D) Raman spectra with 532 nm laser for *t*BN-derived organic films. Top two were obtained in air, with the non-SERS spectrum multiplied by 65. Bottom two spectra are calculated for structures of Scheme 2a, with the predicted intensity of the polaron approximately 10 times that of the reduced form.

grafting, with protonated amines exhibiting binding energies >400 eV.[44,45,47] One feature of note is the lack of an imine (—N═) peak at approximately 398.5 eV in the *t*BN or oxidative spectra. When polyaniline films are grown, the resulting polymer is a mixture of reduced and oxidized nitrogen groups, and this is clearly evident in XPS.[45] The lack of an imine signal for these films suggests that the grafted material contains reduced nitrogen (—NH—/—NH^+—) only. The $NaNO_2$ N 1s scan is clearly different, with deconvolution yielding two peaks, one at 399.2 eV, assigned to —NH— groups, and a second at 400.6 eV that has been assigned to —N═N— (azo) groups, which are often a minor species in diazonium-derived films formed by direct reaction of a diazonium ion.[50,51] This is further evidence to support the

https://dx.doi.org/10.1021/acsami.9b17420
ACS Appl. Mater. Interfaces 2020, 12, 10211−10223

Scheme 2. Proposed Redox Reactions for Singly Bonded 8-Diaminonaphthalene Products for Singly Bridged Nitrogen (2a), Doubly Bridged Nitrogen (2b), and Azo-Coupled Product (2c)

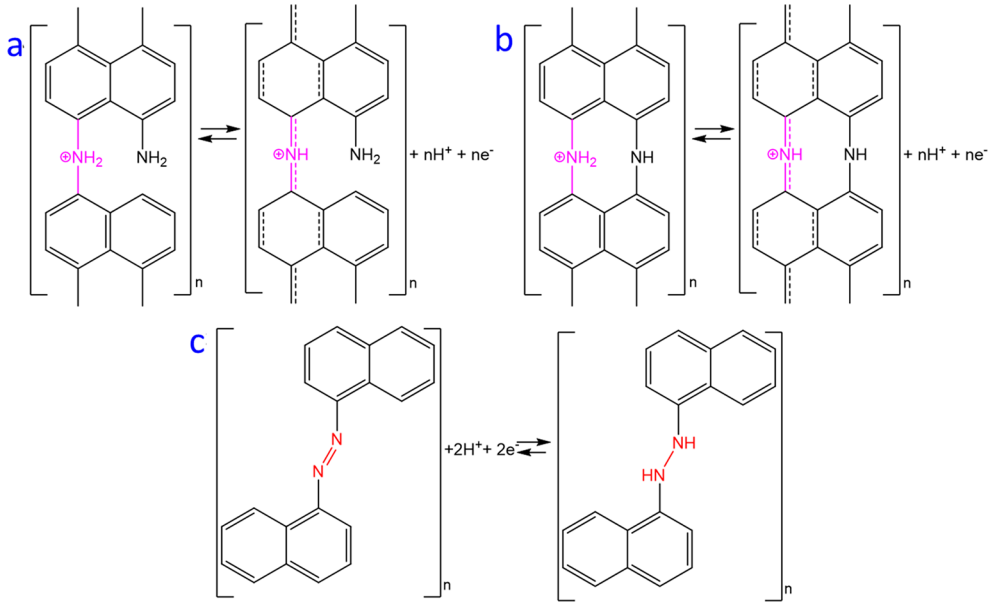

two concurrent grafting mechanisms, i.e., diazonium mediated and oxidative. Given that the possible azo N 1s peak should be divided by two to compare to the —NH— signal, the azo nitrogen is a less prominent component than —NH— nitrogen. The relationship between capacity (determined from C/D and voltammetry between −0.2 and +0.8 V) vs the atom % of nitrogen from XPS is shown in Figure 6C, with the data listed in the Supporting Information, Table S1. The capacity increases for films containing higher nitrogen content, which is expected for an increase in the density of N-containing Faradaic redox centers. The lower capacity values reported for voltammetry are due to the faster scanning rate compared to C/D cycles. Conversely, the EDLC determined from C/D between +0.35 and +0.65 V remains constant despite variation in nitrogen content. The EDLC is a result of the increased surface area and therefore should not be affected by the addition of redox active groups, so this result is expected for films of similar thickness. The charge storage capacity of these films over the −0.2 to +0.8 V potential range can be controlled by changing the nitrogen content of the film, which is dictated by the grafting conditions. Voltammograms similar to those in Figure 1 as a function of solution pH (in McIlvaine buffer) for the three preparation methods are provided in the Supporting Information, Figure S14. The cathodic peak potentials vs pH are shown in Figure 7A for all three preparation procedures (*t*BN, oxidative, and $NaNO_2$), and gradients range from 57 to 62 mV/pH unit, indicating a redox process than involves one proton per electron.

The two redox processes for the $NaNO_2$ film were not well resolved in the pH range 2.6−7.0 buffer, and only a broad redox peak was observed; thus, this was plotted in Figure 6A. The secondary −NH− group shown in the possible structures of Figure 4 is also found in polyaniline made by chemical or electrochemical oxidation of aniline in H_2SO_4 solution.[52−54] Polyaniline has three distinct oxidation states involving this redox center: leucoemeraldine, where the polymer is fully reduced (amine nitrogen groups); emeraldine, with a 50/50 mixture of oxidized and reduced nitrogen; and pernigraniline, where the polymer is fully oxidized (imine nitrogen groups).[53,55] The voltammetry of polyaniline in acidic electrolyte shows redox peaks that correspond to these transitions, in the same potential window as the redox peaks seen for the films studied here.[54,55] Therefore, in agreement with prior work on poly(1,8-DAN) films grown by chemical or electrochemical oxidation,[26,29,31] the redox reaction responsible for the large Faradaic feature in acidic solution is consistent with oxidation of the protonated benzenoid amine to the corresponding quinoid imine, shown schematically in Scheme 2a,b. Further voltammetry in different H_2SO_4 concentrations (0.1, 0.5, and 1 M) exhibits both cathodic peaks (Figure 6B). Both cathodic peaks for the $NaNO_2$ sample shift with pH at ∼59 mV/pH unit (Figure 6A, pink and purple), implying distinct redox reactions with different formal potentials but each involving an equal number of electrons and protons. One can be assigned to the amine/imine process of the *t*BN film and the second to the reaction with a different bonding geometry or the adjacent NH center in Scheme 2b.[56] Alternatively, the redox center responsible for the second peak may be an azo group. Azo linkages can undergo a two proton two electron reduction process to give a diphenylhydrazine species (Scheme 2c).[57,58]

Figure 6C,D illustrates the change in capacity with pH, with all results provided in the Supporting Information, Table S2. Over both potential windows there is a decrease in capacity with increasing pH. The −0.2 to +0.8 V capacity decrease is partially due to the shift in the redox peaks with pH due to displacement of the Faradaic feature studied potential window with increasing pH. In addition, the decrease in capacity with pH may be due to changes in film conductivity, resulting in accessibility of nitrogen redox centers in the organic film. This agrees with previous work on polyaniline and poly(1,8-DAN) films that show that deprotonation generates an insulating layer.[26,53] Indeed, by pH 7 the EDLC is the same (or slightly lower) compared to the unmodified PPF, suggesting an insulating organic layer at neutral pH. Therefore, there are three factors that contribute to the capacity enhancement generated by 1,8-DAN films: the redox behavior caused by nitrogen containing redox active groups (−NH−/−NH^+−),

https://dx.doi.org/10.1021/acsami.9b17420
ACS Appl. Mater. Interfaces 2020, 12, 10211−10223

Table 3. Areal and Normalized Capacity over 1 V Potential Window for PPF/1,8-DAN and Literature Examples

sample	capacity, mC cm^{-2}	thickness, nm	normalized capacity, mC cm^{-2} nm^{-1}	energy storage mechanism	citation
PPF	0.015			EDLC	this work
PPF/1,8-DAN, *t*BN	1.8	15.8	0.11	Faradaic and EDLC	this work
PPF/1,8-DAN, $NaNO_2$	2.9	15.1	0.19	Faradaic and EDLC	this work
PPF/1,8-DAN, oxidative	2.6	16.9	0.15	Faradaic and EDLC	this work
PPF/1,8-DAN with spacers	10.5	22.4	0.47	Faradaic and EDLC	this work
PPF/polyaniline, oxidative	0.083	2.0	0.042	Faradaic and EDLC	this work
activated carbon	0.010−0.025			EDLC	2
graphene ink	6.63	<5000	0.0013	EDLC	61, 62
laser scribed graphene	4.04	<100 000	4.0×10^{-5}	EDLC	63
graphene oxide/polyaniline hydrogel	2300	500 000	0.0046	Faradaic and EDLC	64
polyaniline on stainless steel	64	1200	0.053	Faradaic and EDLC	65
polyaniline on F-doped tin oxide	36	1900	0.019	Faradaic and EDLC	65
polyaniline/graphene stack	326	4500	0.072	Faradaic and EDLC	66

EDLC caused by an increase in the surface area of the electrode, and the improved conductivity of the protonated conducting polymer films.

The possibility that the organic film may retard ion transport and decrease capacity was examined by pretreating the PPF surface before DAN treatment with a sparse layer of pentafluorophenyl "spacers" using a diazonium procedure which did not involve BF_4^- ions.[59,60] As shown in Figure S15, the fluorine coverage preceding DAN treatment from XPS varied from 0.3% to 3%, while the capacity increased from 1.8 to 10.5 C cm^{-2}, a factor of 6× compared to DAN/*t*BN treated PPF and 700× compared to bare PPF (Figure S16). The spacer effect was not examined in detail, but it is clear that fabrication conditions are important to capacity enhancement and provide a further variable for optimization.

Capacity values for the films prepared using the 1,8-DAN precursor on PPF range from 1.8 to 10.5 mC cm^{-2}, as summarized in Table 1. Comparisons to literature values are complicated by large variations in the thickness of the modification layer, and most existing examples of polymer films grafted to conducting substrates involve much thicker films than those used here. Dividing the reported capacity by the layer thickness yields normalized capacity (mC cm^{-2} nm^{-1}), which indicates the density of charge storage sites within the modification layer. Additionally, for Faradaic materials where capacity is the most appropriate metric for describing energy storage, the applied potential window should be constant (in this case 1 V) for comparisons to be informative. Table 3 compares the current PPF-modified surfaces to several distinct modifications of electrodes, including carbon-only electrodes and conducting surfaces modified with polyaniline. Although capacities higher than the PPF-modified surfaces have been reported for thick layers, the PPF/1,8-DAN electrodes have higher charge density, corresponding to approximately 1−2 e^- per naphthalene subunit. The 10−25 nm thick 1,8-DAN modification layers should permit modification of smaller pores and higher surface area substrates, thus increasing the energy storage density of current large surface area supercapacitors. In addition, ion transport through very thin layers is more efficient than in thick layers, resulting in higher power density.

To assess charge/discharge stability, the electrodes prepared in this work were cycled at 1.0 mA cm^{-2} between −0.2 and +0.8 V in 0.1 M H_2SO_4 for 10 000 C/D cycles. Constant current C/D cycles before and after stability testing are provided in the Supporting Information, Figure S18. All surfaces showed impressive stability with no degradation over 10 000 cycles (Figure S17). There was a slight increase in capacity with cycling for the *t*BN and $NaNO_2$ samples, possibly resulting from electrolyte accessing more of the ribbons over time. This stability rivals that of carbon-based EDLC[61,67] and is better than most conducting polymer-based supercapacitors including polypyrrole/reduced graphene oxide composites (39−53% retention after 1000−10 000 cycles),[68,69] graphene/lignin/polyaniline composites (81% retention after 5000 cycles),[70] polyaniline/carbon nanotube films (91% after 10 000 cycles),[71] and nitrogen-doped reduced graphene oxide (91% after 10 000 cycles).[72]

Raman and UV−vis spectroscopy were used previously to characterize organic films formed from 1,8-DAN,[13,15] and the current films were investigated to provide additional evidence for the reactions depicted in Scheme 2. Figure 7B shows UV−vis absorption spectra for films formed by the *t*BN route with 1,8-DAN after subtraction of the absorption by quartz and PPF,[13,15] plus the film formed by the oxidative route without diazotization. Also shown in panel B are predicted spectra for the structure of Scheme 1a and for its polaron form resulting from oxidation (Scheme 2a), with the calculation procedure provided in the Supporting Information, Section 15. Note that only the polaron form has absorption bands above 400 nm and that all three predicted peaks correspond to features in the spectra of Figure 7A. Panel C shows the change in absorbance (ΔA) when the potential of *t*BN formed film is increased from −0.4 to +0.5 V vs Ag/AgCl in 0.1 M H_2SO_4.

The increase in the absorbance bands at ∼540 and ∼750 nm during a positive potential excursion is reversible and repeatable and is consistent with polaron formation during positive potential excursions. The ∼480 nm band in the experimental spectrum of Figure 7A implies that some polaron is present in the as-formed films by both oxidative and *t*BN procedures, consistent with the presence of fluorine indicated by XPS. Normal and surface enhanced Raman (SERS) spectra of films formed by the *t*BN procedure are shown in Figure 7D, using a silver-modified PPF substrate as described previously.[73] The vibrational frequencies are observed values from the SERS spectra, and the lower two spectra of Figure 7D were calculated for the neutral and polaron structures shown in Scheme 2a. Regions of direct interest are the aromatic C═C stretch at 1580−1620 cm^{-1}, the C—N vibrations at 1300−1380, and 1400−1450 bands possibly due to azo N═N stretches or C—NH vibrations. Further support for polaron formation during film oxidation is provided by the in situ SERS

https://dx.doi.org/10.1021/acsami.9b17420
ACS Appl. Mater. Interfaces 2020, 12, 10211−10223

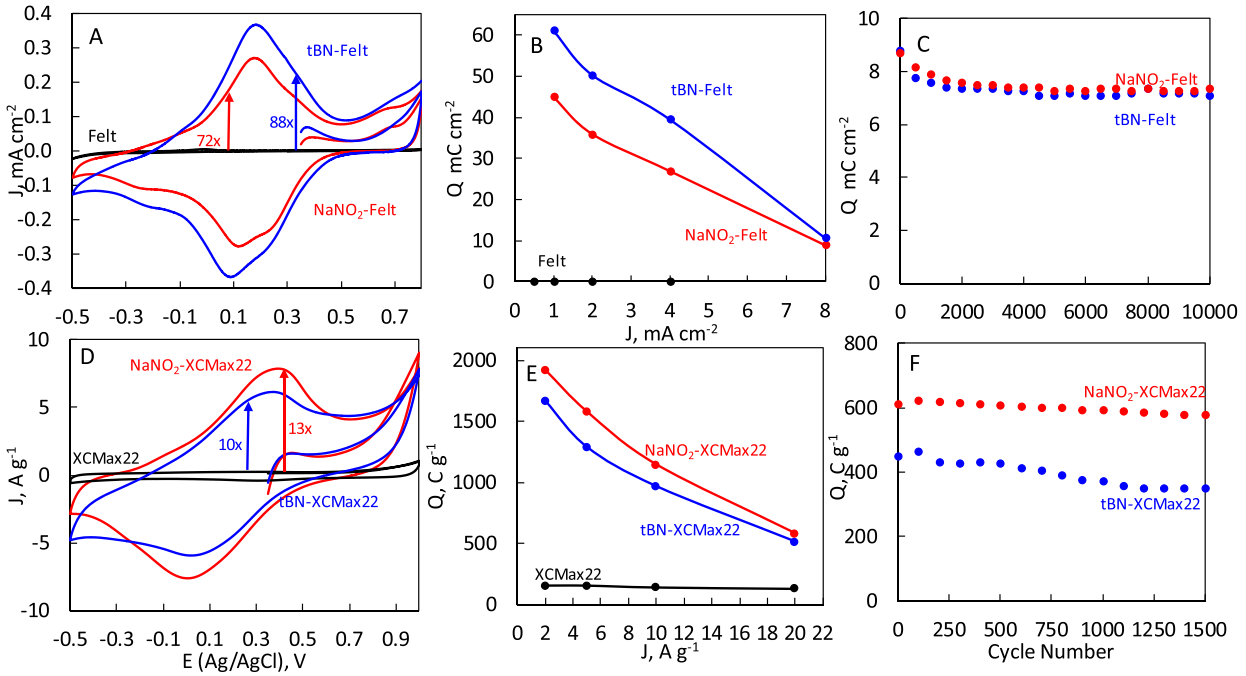

Figure 8. Electrochemistry in 0.1 M H_2SO_4 for high surface area carbons. (A) Voltammetry at 2 mV s^{-1} for carbon felt (black), *t*BN-felt (blue), and $NaNO_2$-felt (red). (B) Capacity calculated from C/D at different applied current densities for carbon felt (black), *t*BN-felt (blue), and $NaNO_2$-felt (red). (C) Change in capacity with prolonged cycling for modified carbon felt determined from C/D cycling at 8 mA cm^{-2} for 10 000 cycles. (D) Voltammetry at 2 mV s^{-1} for XCMax22 (black), *t*BN-XCMax22 (blue), and $NaNO_2$-XCMax22 (red). (E) Capacity calculated from C/D at different applied current densities for XCMax22 (black), *t*BN-XCMax22 (blue), and XCMax22-cloth (red). (F) Change in capacity with prolonged cycling for modified XCMax22 determined by C/D cycling at 20 A g^{-1} for 1500 cycles.

spectroscopy at the center of Figure 7D, during which the applied potential was increased from −0.45 to a positive limit of −0.05 V vs Ag/AgCl due to Ag oxidation. During the positive potential excursion, the C═C stretch shifts from ∼1575 to ∼1615 cm^{-1}, and the intensities of the 1326 and 1365 cm^{-1} features increase significantly. These changes were reversible with repeated potential excursions, with only minor changes of intensity for at least three potential cycles. The ∼1630 cm^{-1} was only predicted for the quinoidal feature of the polaron in Scheme 2a,b, and not for any reduced structures examined. Although the UV−vis absorption and Raman features may be due to structures other than those shown in Scheme 2, the in situ spectroscopic evidence is consistent with a reversible neutral to polaron transition similar to that observed in polyaniline, which likely underlies the large Faradaic component of the capacitance.

Studies on flat carbon substrates like PPF are informative regarding energy storage mechanism and optimization and have possible small-scale applications such as on-chip energy storage. However, for large-scale applications including flexible and wearable electronics, and vehicular and electricity grid applications, much higher surface area and capacity values are required. Figure 8 (and the Supporting Information, Figures S19−S24) shows the *t*BN and $NaNO_2$ 1,8-DAN modifications on two commercially available, high surface area carbon substrates: carbon felt electrodes, and carbon black/steel mesh electrodes using Vulcan XCMax22 carbon black supplied by the Cabot Corporation.

Modification increases the capacity for both high surface area carbons, with a 72−88× increase in capacity for carbon cloth and 10−13X increase in capacity for XCMax22 depending on the modification protocol. The carbon black powder has small pores of 2−5 nm, which are responsible for the high surface area (1360 m^2 g^{-1}), but too small for the 1,8-DAN-derived film (15−17 nm). Conversely, carbon felt has a higher surface area than flat PPF but is not composed of micro- and mesopores like the carbon black powder and thus provides better accessibility for ribbon growth hence an improved capacity enhancement. Using high surface area carbon materials with larger pores may significantly increase capacity, to well above the 10−13× gain observed with XCMax22. In addition to the capacity enhancement, all samples showed little change in the capacity after prolonged cycling, highlighting the impressive stability of electrodes modified with 1,8-DAN.

3. CONCLUSION

Grafting organic films on flat carbon electrodes using aminonaphthalene precursors provides an enhancement in the areal capacity by up to a factor of 700 with film thicknesses of 15−22 nm. To obtain the large capacity enhancement, the 1,8-DAN precursor was essential, with other aminonaphthalene precursors providing reduced enhancements or even decreasing the capacity compared to unmodified PPF. When *t*BN is present in the grafting solution the film grows primarily via an oxidative mechanism, with −NH− linkers in either a one- or two-point binding configuration, providing a nitrogen-doped ribbon structure. Conversely, using $NaNO_2$ as the oxidizing agent enables both the oxidative and diazonium routes to occur and yields increased capacity over the *t*BN procedure. Additionally, the use of aqueous acidic grafting conditions makes this protocol more environmentally friendly, less expensive, and more amenable to industrial processing. The large capacity increase results from both an increase in microscopic area and a larger contribution from Faradaic

https://dx.doi.org/10.1021/acsami.9b17420
ACS Appl. Mater. Interfaces 2020, 12, 10211−10223

processes derived from redox active −NH− groups incorporated in the modification layer. The charge storage density in 1,8-DAN films exceeds that of many existing alternatives, and the <25 nm film thickness should provide efficient ion transport in porous electrode materials. Furthermore, all surfaces showed impressive stability, with little or no degradation after 10 000 C/D cycles. The capacity of the *t*BN film was further enhanced by pregrafting a pentafluorophenyl layer to give a 700× increase in the areal capacity compared to unmodified PPF. Additionally, the modification was successfully applied to high surface area carbon materials (carbon felt and carbon black powder), resulting in capacity enhancements of up to 88× depending on the modification protocol and type of carbon. Incorporation of these electrodes into real-world devices may enable high energy density materials, prepared via a simple solution-based process, using environmentally safe chemicals such as $NaNO_2$ and water.

4. EXPERIMENTAL METHODS

Several modification procedures and experimental measurements have been described previously.[13−15,24] Details of fabrication conditions and procedures used in the current work are provided in the Supporting Information, Section 1.

■ ASSOCIATED CONTENT

Supporting Information

The Supporting Information is available free of charge at https://pubs.acs.org/doi/10.1021/acsami.9b17420.

Experimental details, electrochemical characterization, AFM images, XPS analysis, and UV/vis spectroscopy of grafting solutions (PDF)

■ AUTHOR INFORMATION

Corresponding Author

Richard L. McCreery − *Department of Chemistry, University of Alberta, Edmonton, Alberta T6G 2G2, Canada;* orcid.org/0000-0002-1320-4331; Phone: +1-780-641-1760; Email: richard.mccreery@ualberta.ca

Authors

Anna K. Farquhar − *Department of Chemistry, University of Alberta, Edmonton, Alberta T6G 2G2, Canada;* orcid.org/0000-0003-4156-7567

Scott R. Smith − *Department of Chemistry, University of Alberta, Edmonton, Alberta T6G 2G2, Canada;* orcid.org/0000-0003-0733-6044

Colin Van Dyck − *Department of Physics, University of Mons, 7000 Mons, Belgium;* orcid.org/0000-0003-2853-3821

Complete contact information is available at: https://pubs.acs.org/10.1021/acsami.9b17420

Notes

The authors declare no competing financial interest.

■ ACKNOWLEDGMENTS

This work was supported by the University of Alberta, the National Research Council of Canada, the Natural Sciences and Engineering Research Council, and Alberta Innovates. The authors thank Prof. Daniel Bélanger for his comments regarding capacitance measurements, and John Marsh at Cabot Carbon for the sample of Vulcan XCMax22.

■ REFERENCES

(1) Noori, A.; El-Kady, M. F.; Rahmanifar, M. S.; Kaner, R. B.; Mousavi, M. F. Towards Establishing Standard Performance Metrics for Batteries, Supercapacitors and Beyond. *Chem. Soc. Rev.* **2019**, *48*, 1272−1341.

(2) Zhang, L. L.; Zhao, X. S. Carbon-Based Materials as Supercapacitor Electrodes. *Chem. Soc. Rev.* **2009**, *38*, 2520−2531.

(3) Pech, D.; Brunet, M.; Durou, H.; Huang, P.; Mochalin, V.; Gogotsi, Y.; Taberna, P.-L.; Simon, P. Ultrahigh-Power Micrometre-Sized Supercapacitors Based on Onion-Like Carbon. *Nat. Nanotechnol.* **2010**, *5*, 651.

(4) Miller, J. R.; Simon, P. Electrochemical Capacitors for Energy Management. *Science* **2008**, *321*, 651−652.

(5) Li, X.; Wei, B. Supercapacitors Based on Nanostructured Carbon. *Nano Energy* **2013**, *2*, 159−173.

(6) Deng, Y.; Xie, Y.; Zou, K.; Ji, X. Review on Recent Advances in Nitrogen-Doped Carbons: Preparations and Applications in Supercapacitors. *J. Mater. Chem. A* **2016**, *4*, 1144−1173.

(7) Borenstein, A.; Hanna, O.; Attias, R.; Luski, S.; Brousse, T.; Aurbach, D. Carbon-Based Composite Materials for Supercapacitor Electrodes: A Review. *J. Mater. Chem. A* **2017**, *5*, 12653−12672.

(8) Pognon, G.; Cougnon, C.; Mayilukila, D.; Bélanger, D. Catechol-Modified Activated Carbon Prepared by the Diazonium Chemistry for Application as Active Electrode Material in Electrochemical Capacitor. *ACS Appl. Mater. Interfaces* **2012**, *4*, 3788−3796.

(9) Laheäär, A.; Przygocki, P.; Abbas, Q.; Béguin, F. Appropriate Methods for Evaluating the Efficiency and Capacitive Behavior of Different Types of Supercapacitors. *Electrochem. Commun.* **2015**, *60*, 21−25.

(10) Balducci, A.; Belanger, D.; Brousse, T.; Long, J. W.; Sugimoto, W. Perspective—a Guideline for Reporting Performance Metrics with Electrochemical Capacitors: From Electrode Materials to Full Devices. *J. Electrochem. Soc.* **2017**, *164*, A1487−A1488.

(11) Ke, Q.; Wang, J. Graphene-Based Materials for Supercapacitor Electrodes − a Review. *Journal of Materiomics* **2016**, *2*, 37−54.

(12) Huang, P.; Lethien, C.; Pinaud, S.; Brousse, K.; Laloo, R.; Turq, V.; Respaud, M.; Demortière, A.; Daffos, B.; Taberna, P. L.; Chaudret, B.; Gogotsi, Y.; Simon, P. On-Chip and Freestanding Elastic Carbon Films for Micro-Supercapacitors. *Science* **2016**, *351*, 691−695.

(13) Farquhar, A. K.; Supur, M.; Smith, S. R.; van Dyck, C.; McCreery, R. L. Hybrid Graphene Ribbon/Carbon Electrodes for High-Performance Energy Storage. *Adv. Energy Mater.* **2018**, *8*, 1802439.

(14) Ranganathan, S.; McCreery, R. L. Electroanalytical Performance of Carbon Films with near-Atomic Flatness. *Anal. Chem.* **2001**, *73*, 893−900.

(15) Supur, M.; Van Dyck, C.; Bergren, A. J.; McCreery, R. L. Bottom-up, Robust Graphene Ribbon Electronics in All-Carbon Molecular Junctions. *ACS Appl. Mater. Interfaces* **2018**, *10*, 6090−6095.

(16) Baranton, S.; Bélanger, D. Electrochemical Derivatization of Carbon Surface by Reduction of in Situ Generated Diazonium Cations. *J. Phys. Chem. B* **2005**, *109*, 24401−24410.

(17) Baranton, S.; Bélanger, D. In Situ Generation of Diazonium Cations in Organic Electrolyte for Electrochemical Modification of Electrode Surface. *Electrochim. Acta* **2008**, *53*, 6961−6967.

(18) Chamoulaud, G.; Belanger, D. Spontaneous Derivatization of a Copper Electrode with in Situ Generated Diazonium Cations in Aprotic and Aqueous Media. *J. Phys. Chem. C* **2007**, *111*, 7501−7507.

(19) Fluteau, T.; Bessis, C.; Barraud, C.; Della Rocca, M. L.; Martin, P.; Lacroix, J.-C.; Lafarge, P. Tuning the Thickness of Electrochemically Grafted Layers in Large Area Molecular Junctions. *J. Appl. Phys.* **2014**, *116*, 114509.

(20) Brousse, T.; Bélanger, D.; Long, J. W. To Be or Not to Be Pseudocapacitive? *J. Electrochem. Soc.* **2015**, *162*, A5185−A5189.

(21) Gogotsi, Y.; Penner, R. M. Energy Storage in Nanomaterials − Capacitive, Pseudocapacitive, or Battery-Like? *ACS Nano* **2018**, *12*, 2081−2083.

(22) Li, L.; Secor, E. B.; Chen, K.-S.; Zhu, J.; Liu, X.; Gao, T. Z.; Seo, J.-W. T.; Zhao, Y.; Hersam, M. C. High-Performance Solid-State Supercapacitors and Microsupercapacitors Derived from Printable Graphene Inks. *Adv. Ener. Mater.* **2016**, *6*, 1600909.
(23) Liu, L.; Wang, X.; Izotov, V.; Havrykov, D.; Koltsov, I.; Han, W.; Zozulya, Y.; Linyucheva, O.; Zahorodna, V.; Gogotsi, O.; Gogotsi, Y. Capacitance of Coarse-Grained Carbon Electrodes with Thickness up to 800 Mm. *Electrochim. Acta* **2019**, *302*, 38−44.
(24) Anariba, F.; DuVall, S. H.; McCreery, R. L. Mono- and Multilayer Formation by Diazonium Reduction on Carbon Surfaces Monitored with Atomic Force Microscopy "Scratching. *Anal. Chem.* **2003**, *75*, 3837−3844.
(25) Palys, B. J.; Bukowska, J.; Jackowska, K. Sers of 1,8-Diaminonaphthalene on Gold, Silver and Copper Electrodes Polymerisation and Complexes Formed with the Electrode Material. *J. Electroanal. Chem.* **1997**, *428*, 19−24.
(26) Majid, S.; Rhazi, M. E.; Amine, A.; Curulli, A.; Palleschi, G. Carbon Paste Electrode Bulk-Modified with the Conducting Polymer Poly(1,8-Diaminonaphthalene): Application to Lead Determination. *Microchim. Acta* **2003**, *143*, 195−204.
(27) Li, X.-G.; Huang, M.-R.; Li, S.-X. Facile Synthesis of Poly(1,8-Diaminonaphthalene) Microparticles with a Very High Silver-Ion Adsorbability by a Chemical Oxidative Polymerization. *Acta Mater.* **2004**, *52*, 5363−5374.
(28) Tagowska, M.; Pałys, B.; Mazur, M.; Skompska, M.; Jackowska, K. In Situ Deposition of Poly(1,8-Diaminonaphthalene): From Thin Films to Nanometer-Sized Structures. *Electrochim. Acta* **2005**, *50*, 2363−2370.
(29) Lee, J. W.; Park, D. S.; Shim, Y. B.; Park, S. M. Electrochemical Characterization of Poly(1,8-Diaminonaphthalene): A Functionalized Polymer. *J. Electrochem. Soc.* **1992**, *139*, 3507−3514.
(30) Oyama, N.; Sato, M.; Ohsaka, T. Preparation of Thin Polymeric Films on Electrode Surfaces by Electro-Polymerization of Aromatic Compounds with Amino Groups. *Synth. Met.* **1989**, *29*, 501−506.
(31) Skompska, M.; Hillman, A. R. Electrochemical Quartz Crystal Microbalance Studies of the Electropolymerization, Electroactivity and Complexing Properties of Poly(1,8-Diaminonaphthalene) Films. *J. Chem. Soc., Faraday Trans.* **1996**, *92*, 4101−4108.
(32) Jackowska, K.; Skompska, M.; Przyłuska, E. Electro-Oxidation of 1,5 and 1,8 Diaminonaphthalene: An Rde Study. *J. Electroanal. Chem.* **1996**, *418*, 35−39.
(33) Blond, P.; Mattiuzzi, A.; Valkenier, H.; Troian-Gautier, L.; Bergamini, J.-F.; Doneux, T.; Goormaghtigh, E.; Raussens, V.; Jabin, I. Grafting of Oligo(Ethylene Glycol)-Functionalized Calix[4]Arene-Tetradiazonium Salts for Antifouling Germanium and Gold Surfaces. *Langmuir* **2018**, *34*, 6021−6027.
(34) Torréns, M.; Ortiz, M.; Turner, A. P. F.; Beni, V.; O'Sullivan, C. K. Controlled Zn-Mediated Grafting of Thin Layers of Bipodal Diazonium Salt on Gold and Carbon Substrates. *Chem. - Eur. J.* **2015**, *21*, 671−681.
(35) Harnisch, J. A.; Gazda, D. B.; Anderegg, J. W.; Porter, M. D. Chemical Modification of Carbonaceous Stationary Phases by the Reduction of Diazonium Salts. *Anal. Chem.* **2001**, *73*, 3954−3959.
(36) Downard, A. J. Potential-Dependence of Self-Limited Films Formed by Reduction of Aryldiazonium Salts at Glassy Carbon Electrodes. *Langmuir* **2000**, *16*, 9680−9682.
(37) Laforgue, A.; Addou, T.; Bélanger, D. Characterization of the Deposition of Organic Molecules at the Surface of Gold by the Electrochemical Reduction of Aryldiazonium Cations. *Langmuir* **2005**, *21*, 6855−6865.
(38) Yu, D. S.; Kuila, T.; Kim, N. H.; Lee, J. H. Enhanced Properties of Aryl Diazonium Salt-Functionalized Graphene/Poly(Vinyl Alcohol) Composites. *Chem. Eng. J.* **2014**, *245*, 311−322.
(39) Vettorazzi, N.; Silber, J. J.; Sereno, L. Solvent Effects in Electrochemical Oxidation of 1-Naphthylamine: Dimethylsulfoxide Vs. Acetonitrile. *J. Electroanal. Chem. Interfacial Electrochem.* **1983**, *158*, 89−102.
(40) Arévalo, A. H.; Fernández, H.; Silber, J. J.; Sereno, L. Mechanism of Electropolymerization of 1-Naphthylamine in Aqueous Acid Media. *Electrochim. Acta* **1990**, *35*, 741−748.
(41) Jin, C.-S.; Shim, Y.-B.; Park, S.-M. Electropolymerization and Spectroelectrochemical Characterization of Poly(1,5-Diaminonaphthalene). *Synth. Met.* **1995**, *69*, 561−562.
(42) Ruangchuay, L.; Schwank, J.; Sirivat, A. Surface Degradation of A-Naphthalene Sulfonate-Doped Polypyrrole During Xps Characterization. *Appl. Surf. Sci.* **2002**, *199*, 128−137.
(43) Choukourov, A.; Kousal, J.; Slavínská, D.; Biederman, H.; Fuoco, E. R.; Tepavcevic, S.; Saucedo, J.; Hanley, L. Growth of Primary and Secondary Amine Films from Polyatomic Ion Deposition. *Vacuum* **2004**, *75*, 195−205.
(44) Li, Q.; Qian, Y.; Cui, H.; Zhang, Q.; Tang, R.; Zhai, J. Preparation of Poly(Aniline-1,8-Diaminonaphthalene) and Its Application as Adsorbent for Selective Removal of Cr(Vi) Ions. *Chem. Eng. J.* **2011**, *173*, 715−721.
(45) Kumar, S. N.; Gaillard, F.; Bouyssoux, G.; Sartre, A. High-Resolution Xps Studies of Electrochemically Synthesized Conducting Polyaniline Films. *Synth. Met.* **1990**, *36*, 111−127.
(46) Meneguzzi, A.; Pham, M. C.; Lacroix, J.-C.; Piro, B.; Adenier, A.; Ferreira, C. A.; Lacaze, P.-C. Electroactive Poly(Aromatic Amine) Films for Iron Protection in Sulfate Medium. *J. Electrochem. Soc.* **2001**, *148*, B121−B126.
(47) Kang, E. T.; Neoh, K. G.; Tan, K. L.; Tan, B. T. G. Protonation of the Amine Nitrogens in Emeraldine — Evidence from X-Ray Photoelectron Spectroscopy. *Synth. Met.* **1992**, *46*, 227−233.
(48) Li, X.-G.; Huang, M.-R.; Duan, W.; Yang, Y.-L. Novel Multifunctional Polymers from Aromatic Diamines by Oxidative Polymerizations. *Chem. Rev.* **2002**, *102*, 2925−3030.
(49) Snauwaert, P.; Lazzaroni, R.; Riga, J.; Verbist, J.; Gonbeau, D. A Photoelectron Spectroscopic Study of the Electrochemical Processes in Polyaniline. *J. Chem. Phys.* **1990**, *92*, 2187−2193.
(50) Doppelt, P.; Hallais, G.; Pinson, J.; Podvorica, F.; Verneyre, S. Surface Modification of Conducting Substrates. Existence of Azo Bonds in the Structure of Organic Layers Obtained from Diazonium Salts. *Chem. Mater.* **2007**, *19*, 4570−4575.
(51) Yu, S. S. C.; Tan, E. S. Q.; Jane, R. T.; Downard, A. J. An Electrochemical and Xps Study of Reduction of Nitrophenyl Films Covalently Grafted to Planar Carbon Surfaces. *Langmuir* **2007**, *23*, 11074−11082.
(52) Huang, W.-S.; Humphrey, B. D.; MacDiarmid, A. G. Polyaniline, a Novel Conducting Polymer. Morphology and Chemistry of Its Oxidation and Reduction in Aqueous Electrolytes. *J. Chem. Soc., Faraday Trans. 1* **1986**, *82*, 2385−2400.
(53) Gospodinova, N.; Terlemezyan, L. Conducting Polymers Prepared by Oxidative Polymerization: Polyaniline. *Prog. Polym. Sci.* **1998**, *23*, 1443−1484.
(54) Zhang, J.; Kong, L.-B.; Wang, B.; Luo, Y.-C.; Kang, L. In-Situ Electrochemical Polymerization of Multi-Walled Carbon Nanotube/Polyaniline Composite Films for Electrochemical Supercapacitors. *Synth. Met.* **2009**, *159*, 260−266.
(55) Wang, Q.; Li, J.-l.; Gao, F.; Li, W.-s.; Wu, K.-z.; Wang, X.-d. Activated Carbon Coated with Polyaniline as an Electrode Material in Supercapacitors. *New Carbon Materials* **2008**, *23*, 275−280.
(56) Abiman, P.; Wildgoose, G. G.; Compton, R. G. Investigating the Mechanism for the Covalent Chemical Modification of Multiwalled Carbon Nanotubes Using Aryl Diazonium Salts. *Int. J. Electrochem. Sci.* **2008**, *3*, 104−117.
(57) Jung, H. J.; Min, H.; Yu, H.; Lee, T. G.; Chung, T. D. Electrochemical Cleavage of Azo Linkage for Site-Selective Immobilization and Cell Patterning. *Chem. Commun.* **2010**, *46*, 3863−3865.
(58) Sadowska, K.; Roberts, K. P.; Wiser, R.; Biernat, J. F.; Jabłonowska, E.; Bilewicz, R. Synthesis, Characterization, and Electrochemical Testing of Carbon Nanotubes Derivatized with Azobenzene and Anthraquinone. *Carbon* **2009**, *47*, 1501−1510.
(59) Farquhar, A. K.; Dykstra, H. M.; Waterland, M. R.; Downard, A. J.; Brooksby, P. A. Spontaneous Modification of Free-Floating Few-Layer Graphene by Aryldiazonium Ions: Electrochemistry, Atomic

https://dx.doi.org/10.1021/acsami.9b17420
ACS Appl. Mater. Interfaces 2020, 12, 10211−10223

Force Microscopy, and Infrared Spectroscopy from Grafted Films. *J. Phys. Chem. C* **2016**, *120*, 7543−7552.
(60) Mesnage, A.; Lefèvre, X.; Jégou, P.; Deniau, G.; Palacin, S. Spontaneous Grafting of Diazonium Salts: Chemical Mechanism on Metallic Surfaces. *Langmuir* **2012**, *28*, 11767−11778.
(61) Hyun, W. J.; Secor, E. B.; Kim, C.-H.; Hersam, M. C.; Francis, L. F.; Frisbie, C. D. Scalable, Self-Aligned Printing of Flexible Graphene Micro-Supercapacitors. *Adv. Ener. Mater.* **2017**, *7*, 1700285.
(62) Song, D.; Secor, E. B.; Wang, Y.; Hersam, M. C.; Frisbie, C. D. Transfer Printing of Sub-5 Mm Graphene Electrodes for Flexible Microsupercapacitors. *ACS Appl. Mater. Interfaces* **2018**, *10*, 22303−22310.
(63) El-Kady, M. F.; Strong, V.; Dubin, S.; Kaner, R. B. Laser Scribing of High-Performance and Flexible Graphene-Based Electrochemical Capacitors. *Science* **2012**, *335*, 1326.
(64) Guo, G.; Sun, Y.; Ma, Y.; Zhou, Y.; Xiong, Z.; Liu, Y. Facile Synthesis of Conducting Hydrogels Based on Polyaniline Fiber and Graphene Oxide for Application in All-Solid-State Supercapacitors. *Int. J. Electrochem. Sci.* **2019**, *14*, 5899−5912.
(65) Deshmukh, P.; Shinde, N. M.; Patil, S.; Bulakhe, R.; Lokhande, C. Supercapacitive Behavior of Polyaniline Thin Films Deposited on Fluorine Doped Tin Oxide (Fto) Substrates by Microwave-Assisted Chemical Route. *Chem. Eng. J.* **2013**, *223*, 572−577.
(66) Wu, Z.-S.; Parvez, K.; Li, S.; Yang, S.; Liu, Z.; Liu, S.; Feng, X.; Müllen, K. Alternating Stacked Graphene-Conducting Polymer Compact Films with Ultrahigh Areal and Volumetric Capacitances for High-Energy Micro-Supercapacitors. *Adv. Mater.* **2015**, *27*, 4054−4061.
(67) Song, D.; Zare Bidoky, F.; Secor, E. B.; Hersam, M. C.; Frisbie, C. D. Freestanding Ion Gels for Flexible, Printed, Multifunctional Microsupercapacitors. *ACS Appl. Mater. Interfaces* **2019**, *11*, 9947−9954.
(68) Hamra, A. A. B.; Lim, H. N.; Hafiz, S. M.; Kamaruzaman, S.; Rashid, S. A.; Yunus, R.; Altarawneh, M.; Jiang, Z. T.; Huang, N. M. Performance Stability of Solid-State Polypyrrole-Reduced Graphene Oxide-Modified Carbon Bundle Fiber for Supercapacitor Application. *Electrochim. Acta* **2018**, *285*, 9−15.
(69) Guo, M.; Zhou, Y.; Sun, H.; Zhang, G.; Wang, Y. Interconnected Polypyrrole Nanostructure for High-Performance All-Solid-State Flexible Supercapacitor. *Electrochim. Acta* **2019**, *298*, 918−923.
(70) Wu, D.; Zhong, W. A New Strategy for Anchoring a Functionalized Graphene Hydrogel in a Carbon Cloth Network to Support a Lignosulfonate/Polyaniline Hydrogel as an Integrated Electrode for Flexible High Areal-Capacitance Supercapacitors. *J. Mater. Chem. A* **2019**, *7*, 5819−5830.
(71) Gao, D.; Liu, R.; Yu, W.; Luo, Z.; Liu, C.; Fan, S. Gravity-Induced Self-Charging in Carbon Nanotube/Polymer Supercapacitors. *J. Phys. Chem. C* **2019**, *123*, 5249−5254.
(72) Dang, F.; Yang, P.; Zhao, W.; Liu, J. Z.; Wu, H.; Liu, A.; Liu, Y. Tuning Capacitance of Graphene Films Via a Robust Routine of Adjusting Their Hierarchical Structures. *Electrochim. Acta* **2019**, *298*, 254−264.
(73) Supur, M.; Smith, S. R.; McCreery, R. L. Characterization of Growth Patterns of Nanoscale Organic Films on Carbon Electrodes by Surface Enhanced Raman Spectroscopy. *Anal. Chem.* **2017**, *89*, 6463−6471.

https://dx.doi.org/10.1021/acsami.9b17420
ACS Appl. Mater. Interfaces 2020, 12, 10211−10223